Development and airborne operation of a compact water isotope ratio infrared spectrometer

Rosario Iannone, Samir Kassi, Hans-Jürg Jost, Marc Chenevrier, D. Romanini, Harro A.J. Meijer, Suresh Dhaniyala, Marcel Snels, E. R. T. Kerstel

Development and airborne operation of a compact water isotope ratio infrared spectrometer

Rosario Q. Iannone [1], Samir Kassi [2], Hans-Jürg Jost [3], Marc Chenevier [2], Daniele Romanini [2], Harro A. J. Meijer [1], Suresh Dhaniyala [4], Marcel Snels [5], and Erik R. T. Kerstel [1, 2]

[1] Centrum voor IsotopenOnderzoek (CIO), University of Groningen, 9747 AG Groningen, The Netherlands

[2] Laboratoire de Spectrométrie Physique CNRS UMR5588, J. Fourier University of Grenoble, Saint Martin d'Hères, France

[3] NovaWave Technologies, Redwood City, CA 94065, USA

[4] Clarkson University, Mechanical and Aeronautical Engineering, Potsdam NY 13699, USA

[5] Institute of Atmospheric Sciences and Climate - CNR, 00133 Rome, Italy

email: erik.kerstel@ujf-grenoble.fr

Abstract

A sensitive laser spectrometer, named IRIS, was developed for the *in situ* detection of the isotopic composition of water vapor in the upper troposphere and the lower stratosphere. Isotope ratio measurements can be used to quantify troposphere-stratosphere exchange, and to study the water chemistry in the stratosphere. IRIS is based on the technique of optical-feedback cavity enhanced absorption spectroscopy. It uses a room temperature near-infrared laser, and does not require cryogenic cooling of laser or detectors. The instrument weighs 51 kg including its support structure. Airborne operation was demonstrated during three flights aboard of the European M55-Geophysica stratospheric research aircraft, as part of the AMMA/SCOUT-03 (African Monsoon Multidisciplinary Analysis/Stratospheric Climate links with emphasis on the Upper Troposphere and lower stratosphere) campaign in Burkina Faso in August 2006. One-second averaged, vertical profiles of δ^2H, $\delta^{17}O$, and $\delta^{18}O$ in the upper troposphere are shown, as are the $\delta^{17}O$-$\delta^{18}O$ and δ^2H-$\delta^{18}O$ relations. The data are discussed with reference to a Raleigh distillation model. As expected in the troposphere, there is no indication of non-mass dependent fractionation (also known as mass independent fractionation).

Furthermore, improvements to the thermal management system and a move to a (cryogen-free) longer wavelength laser source are discussed, which together should result in an approximately two orders of magnitude improvement of the sensitivity.

Keywords: water vapor isotopes, airborne, troposphere-stratosphere exchange, in-situ infrared laser spectroscopy, optical feedback cavity enhanced absorption spectroscopy; OF-CEAS; mass independent fractionation; MIF.

1. Introduction

Recent years have seen an increasing interest in water vapor in the upper troposphere and lower stratosphere (UTLS), and in the stratosphere-troposphere exchange (STE) processes in particular. This is because water participates in chemical reactions and shows spatial inhomogeneity, both complicating the estimation of the net mass flux. In the stratosphere, the distribution of water vapor can be explained as a balance between very low humidity air entering via the tropical tropopause and a local source of water vapor obtained from methane oxidation. Observations show a multi-decadal increase in water vapor in the stratosphere that, however, cannot be explained by the rise of tropospheric methane. Rather, this increase, which is radiatively significant, is attributed to circulation changes [1]. Forster and Shine [2] emphasized that an increase of water vapor may produce a cooling of the lower stratosphere, thus impacting the stratospheric chemistry. Modeling studies suggest that increased water vapor concentrations will enhance odd hydrogen (HOx) in the stratosphere and subsequently influence ozone depletion. Increases in water vapor in polar regions would raise the temperature threshold for the formation of polar stratospheric clouds, potentially increasing springtime ozone depletion [3].

Understanding mechanisms of water vapor transport will consequently add to a better understanding of the climate system, and our ability to predict future climate changes. Unfortunately, measuring water vapor in the lower stratosphere is not easy considering that the stratosphere is exceedingly arid, with a mixing ratio of only ~4 ppmv in the annual mean [4]. Hence, progress in our understanding of the mechanisms that control atmospheric water vapor transport between the troposphere and the stratosphere has been slow.

In the last years, it has been demonstrated that the isotopic composition of water vapor can be exploited to better distinguish the pathways of water into the stratosphere and to improve quantification of the associated transport processes [5-12]. The isotopic composition of atmospheric water provides information about its origin that cannot be determined from concentration measurements alone.

The Rayleigh distillation model has been successfully used to describe the variations in water isotopic composition in the lower troposphere [13-15]. If one assumes, as is implicit in the Rayleigh model, that all condensate, once formed, is removed without any significant evaporation, a value of δ^2H = -900‰ in the stratosphere is expected [16]. To explain such extreme depletion of stratospheric air, Holton and Gettelman [16] proposed a so-called gradual dehydration process, in which the isotopic composition of moisture entering the stratosphere is regulated by the coldest tropopause temperature experienced during horizontal movement of air parcels. However, measurements of water vapor isotopes show that the lower stratosphere is isotopically heavier than what is predicted by Rayleigh distillation. Remote sensing observations indicate, in fact, an annual average value of δ^2H=-650‰ in the lower to mid-stratosphere [6, 9]. Convection and cloud microphysics are the key ingredients of a second theory, known as convective dehydration [8]. This convection theory supposes that stratospheric entry depletion for δ^2H is roughly -650‰.

So far, relatively few data have been collected and these observations are sparse in both space and time. The absence of long-term observations of water vapor isotopologues in the tropical tropopause layer (TTL) makes it impossible to study seasonal effects. High spatial resolution is essential to be able to investigate STE mechanisms. Data integration between space observation and in-situ measurements

using aircraft, balloons and lidar is critical if we want to be able to use these data with confidence to test theoretical models. In-situ measurements carried out on aircraft platforms not only provide the high resolution needed to study the issues related to global climate change and atmospheric chemistry, but they are also a critical part of satellite validation and confirmation of models applied to remote sensing measurements.

To date, only two attempts have been made to make in-situ, continuous measurements using spectroscopic detection on an aircraft platform.

Late 2003, Webster and Heymsfield [17] published $^{1}HO^{2}H$ isotope signals between 0 and -900‰, obtained with an in-situ infrared laser spectrometer (ALIAS) during a NASA campaign in 2002. These very negative values near –900‰ could indicate that one of the predominant entry mechanisms of water vapor is given by a gradual ascent of air towards the stratosphere. It is worth noting, however, that the Webster and Heymsfield [17] data show very large isotopic variations not generally seen with other in-situ aircraft-based measurements [18], aircraft-based cryogenic sampling [19, 20], balloon-based measurements [9], and satellite remote sensing [6, 11, 21]. Recent in-situ measurements carried out by Hanisco and colleagues [18] show much lower depletion values than the data of Webster and Heymsfeld, with an isotopic signal for $\delta^{2}H$ of about -600‰ near the tropopause (~12 km) and increasing again to about -400‰ at higher altitude (~20 km), indicating that in this case gradual dehydration cannot be the only cause of dehydration in the TTL, and that instead convective overshooting influences the isotopic composition of water in stratospheric air. The ~200‰ difference with the observed values at higher altitude is explained by ice lofting [7]. In the particular case of Hanisco et al. [18], the observation of a $\delta^{2}H$ = -

450‰ indicates that a large fraction (~45%) of this lofted ice remains in the stratosphere and subsequently evaporates, in order to make a significant contribution to the total moisture content and the isotopic enrichment of stratospheric water. Despite that, Dessler and Sherwood [10] have remarked that the structure of the vertical profile of δ^2H in the TTL is more relevant than the final value observed if it comes to deciding which theory best fits the data.

Webster and Heymsfeld [17] used a mid-infrared, wavelength modulated quantum cascade laser (QCL) spectrometer with a 1-m base length, 80-pass cell. The spectrometer employed by the Anderson group at Harvard [18] also uses a cryogenically cooled QCL near 6.7 μm, but achieves a much larger effective optical absorption path length (~ 4.5 km) by the use of a derivative of the technique of cavity ring down spectroscopy (CRDS), in this case named Off-Axis Integrated Cavity Output Spectroscopy (OA-ICOS) [22, 23]. Both instruments were flown on the NASA WB57 stratospheric aircraft. As all CRDS techniques, apart from the long path length, OA-ICOS has the advantage of a very large dynamic range, since its sensitivity, dictated by the ring down time, decreases with increasing sample optical density. The longer absorption path length and increased sensitivity of the OA-ICOS instrument comes at a price: In order to effectively suppress noise due to spurious optical resonances in the cavity, large diameter mirrors are needed to reduce overlap between neighboring beam spots on the cavity mirrors. In fact, due to the long wavelength, 10 cm diameter mirrors were required for the 1-m base length cavity. This in turn required a large pump to obtain a sufficiently fast gas exchange. Furthermore, the mid-infrared laser and detectors require liquid nitrogen to operate. The consequence is a heavy and sizeable instrument, which takes up a significant part of the payload.

It has been our aim to develop a sensitive, but compact and lightweight spectrometer without a need for cryogen cooling. As such, the spectrometer can be more easily integrated on different research platforms, potentially including unmanned aerial vehicles (UAVs). The instrument was named IRIS, for water Isotope Ratio Infrared Spectrometer, and has been described previously [24]. IRIS uses the technique of optical feedback cavity enhanced absorption spectroscopy (OF-CEAS) [25] to obtain an effective optical absorption path length of about 6 km for the measurement of deuterium and oxygen isotope ratios in water in the upper troposphere and lower stratosphere. OF-CEAS enables the construction of a very compact device with a small gas cell volume. The small gas cell volume of ~10 mL assures a fast gas cell exchange (< 3 to 4 s) with a very modest pumping speed (~150 mL/min). The high gas exchange rate is also critical in avoiding systematic errors due to contamination by tropospheric water.

IRIS was integrated and flew for the first time on the European Geophysica aircraft as part of the AMMA/SCOUT-03 campaign in the months of July and August 2006, in Ouagadougou, Burkina Faso. AMMA (African Monsoon Multidisciplinary Analysis) is an international project that aims to answer fundamental scientific questions concerning the West African monsoon, while SCOUT-03's (Stratospheric Climate links with emphasis on the Upper Troposphere and lower stratosphere) aim is to provide predictions about the evolution of the coupled chemistry/climate system, with emphasis on ozone change in the lower stratosphere and the associated UV and

climate impact[1]. Measurements of water vapor isotopes, enabling the identification of convective turrets in the TTL, are extremely relevant to both projects. It is worth noting that central Africa represents an excellent location to carry out this kind of measurement since the region in the deep tropics (15º N–15º S) and centered around an altitude of ~10 km (> 340 K potential temperature) is associated with convective outflow at the top of the tropical Hadley circulation, and is one of the dominant regions where final dehydration of tropospheric air takes place [26].

In addition to the goals explained above, a secondary goal was to perform needed intercomparison measurements of water vapor isotopes by comparing our spectrometer to an independent technique mounted on the same aircraft. In this case, we wanted to compare the time-series obtained by our instrument with the off-line, low time resolution, but potentially more precise, whole air cryogenic sampling (WAS) device [27] of the group of Röckmann of Utrecht University. Such an inter-comparison between two fundamentally different measurement techniques is of obvious great importance to assess the quality of the data. More importantly, the combination of the two devices would enable us to construct a high temporal resolution data set, calibrated with simultaneously sampled, but laboratory analyzed water isotope measurements. Unfortunately, to date no data are available from the WAS instrument because of contamination of the samples during transport from Africa to Europe.

2. Instrument Description

[1] The AMMA/SCOUT-03 campaign was funded by the European Union under grant 4089. On the basis of a French initiative, AMMA was built by an international scientific group and is currently funded by a large number of agencies, especially from France, the UK, the USA, and Africa. It has been the beneficiary of a major financial contribution from the European Community's Sixth Framework Research Programme. Detailed information on scientific coordination and funding is available on the AMMA International web site http://www.ammainternational.org.

A detailed description of the instrument can be found in a previous publication [24], while the technique of OF-CEAS is described in more detail by Morville et al. [25]. Here we present the essentials, and then specifically those that relate to the integration on the Geophysica airplane.

The OF-CEAS technique solves the problem of an extremely low light throughput, inherent to most other implementations of CRDS or CEAS techniques, by the use of optical feedback from the cavity to the laser source, to automatically lock the laser frequency to a cavity transmission. It has the added advantage that the cavity longitudinal mode structure is used to probe the absorption spectrum at frequencies equally spaced by the cavity free spectral range (150 MHz). There is thus essentially no noise on the frequency scale of the absorption spectra, facilitating a precise fit of the spectral features. The measurement rate is 6 spectral scans per second. The conversion of the spectra to absolute absorption units is made using the ring down time determined for one pre-selected mode in the spectrum, once every 10 spectra. The mathematical approach has been explained in more detail by Kerstel et al. [24].

Physically, IRIS can be divided into 3 subsystems. The first one is the optical head, which includes the DFB diode laser, the optical cavity, and two detectors. At the time the actual development of the spectrometer started in early 2003, room temperature, continuous-wave laser sources were not (commercially) available in the 2.7 μm or 6.7 μm regions covering, respectively, the ν_1/ν_3 and ν_2 fundamental vibrational bands of water. Instead, the instrument uses a near-infrared diode laser emitting near 1.39 μm., exciting roughly one order of magnitude weaker transitions of the $2\nu_2+\nu_3$ combination band. This high-quality distributed feedback laser is based on telecommunications technology and is thus relatively inexpensive and easily available.

The second subsystem concerns the electronic system, which includes a compact PC 104, laser driver, and data acquisition. The third subsystem is the gas flow system including pressure and flow controllers and a scroll pump. Except for the PC104 and the pump, all three subsystems are physically integrated on a breadboard machined from one piece of aluminum, 5 cm thick, 25.5 cm wide, and 65 cm long.

Temperature stability of the optical head is achieved by enclosing the whole optical system in a thermally insulated aluminum case, while the breadboard is heated with several thermo-foil surface heaters (total installed power is 100 W), covering almost the entire bottom of the base plate, and controlled by a simple on/off thermostat set to 31.5 °C. The average power consumption of the entire system is less than 150 W, while the peak power consumption is limited to 260 W (fused). A pressure controller at the entrance of the cavity regulates the pressure inside the cavity. The working pressure of 98 mbar is optimized for measurements in the middle to high troposphere (up to ca. 16 km), while the flow of ~150 mL/min (STP) is controlled by an electro-valve at the exit of the cavity. The maximum flow rate for this system is ~700 mL/min, at which level turbulent flow start to disturb the optical feedback phase control loop. The flow through the spectrometer cavity slowly increases from zero to the set value (150 mL/min), starting at an altitude between 3 and 5 km. Once the correct flow rate has been established, the instrument starts collecting valid data, typically at an altitude of around 7 km. To minimize adsorption effects of water, a hydrophobic coating (Restek Corp.) was applied to the polished steel surfaces of the cavity and its pressure controller.

Adding a dedicated water isotope inlet was beyond the scope of the current mission. Instead an existing inlet, shared with the CO tunable diode laser spectrometer (COLD, ref [28]), was modified to provide a second outlet, which was connected to the IRIS

inlet using coated tubing (O'Brian). The inlet samples the air outside the airplane boundary layer through a 4 mm inner diameter tube oriented perpendicular to the main air flow in the inlet probe [28]. As larger particles cannot make the sharp bend of the streamlines, the probe samples the gas phase only. No part of the inlet and tubing leading to the spectrometer was heated. Inside the spectrometer, a 30 cm long, folded section of tubing is heated to the breadboard temperature. Simulations indicated that, given the flow conditions, this should suffice to fully thermalize the gas before it enters the gas cell.

IRIS was integrated on the Geophysica mounting structure known as CVI-rack, which contains, besides IRIS, the COLD and COPAS-2 (COndensation PArticle detection System – University of Mainz) instruments. The CVI-rack is mounted in Bay II of the aircraft, directly underneath the cockpit. It should be noted that this part of the aircraft is not pressurized or heated, exposing IRIS to low ambient pressure and temperature at high altitude.

The absorption spectra are saved to solid-state disk (CF-memory) for post-flight data processing. The spectra are fit to a sum of a polynomial baseline and Voigt line profiles. Figure 1 shows a typical in-flight spectrum, including model fit and residuals. This spectrum was recorded in a little less than 0.2 s during the flight from Ouagadougou on August 7, at a height of about 10 km and a water mixing ratio of 300 ppmv.

The spectral model fits the spectra with the spectral line positions, line intensities, and Gaussian (Doppler broadening) and Lorentzian (pressure broadening) widths as parameters. The Gaussian width of the lines is fixed to the isotopologue mass-dependent Doppler width at the temperature of the gas in the spectrometer gas cell.

For the spectra at low water mixing ratio (υ < 1500 ppmv), the Lorentzian widths are fixed. These average Lorentzian widths were determined for each spectral line at relatively high mixing ratio (~1500 ppmv) during the pre- and post-campaign calibration of the spectrometer. This makes the fit more robust and leads to a higher level of precision of the isotope ratios. As the total pressure in the gas cell is controlled to a constant value of 98 mbar, and the self-broadening is relatively unimportant compared to the foreign-gas broadening, the Lorentzian width is expected to be independent of the mixing ratio in this case. But, the accurate determination of the total water concentration requires that the line widths are free in the fit of data recorded at an outside pressure below 98 mbar (υ < 30 ppm). The extremely good frequency scale of the spectra allows the relative line positions to be fixed as well. Still, the fit procedure is tolerant of overall frequency drift of the spectrum, as the routine monitors the position of the strongest peak, which is used as the starting value for the absolute position of the spectral lines. The fit thus returns the line intensities in the spectrum, which, in combination with the line width data, are used to analytically calculate the corresponding line areas.

The technique of CEAS yields a direct measurement of the wavelength dependent absorption coefficient a, which can be written as the product of the number density n, the normalized line shape function g, and the line strength S [29]. Integration of the absorption coefficient over the entire line profile (i.e., the 'line area'), directly yields the number density of the associated species, assuming the line strength is known. The line strengths of the absorption lines probed in this study, as well as their temperature and pressure dependencies, are all tabulated in the HITRAN database [29]. The mixing ratio is calculated assuming ideal gas behavior. The isotope ratios, instead, are given by the super-ratio of the absorption coefficients of the rare and abundant

isotopologues in the sample and a reference material, and thus require, in principle, no knowledge of the line strengths [30]. For example, in the case of the ^{18}O isotopologue:

$$\delta^{18}O = \frac{\left(a(H^{18}OH)/a(H^{16}OH)\right)_{sample}}{\left(a(H^{18}OH)/a(H^{16}OH)\right)_{ref}} - 1 \quad (1)$$

The reference material in the case of water is Vienna Standard Mean Ocean Water (VSMOW) [31]. The reference ratio of absorption coefficients is determined experimentally through pre- and post-flight calibration measurements on local standard materials that are well-characterized with respect to VSMOW, as further discussed in the next section.

3. Laboratory measurements and isotope scale calibration

Prior to the campaign the instrument was characterized in terms of linearity of response, as well as precision and accuracy of the isotope measurements. This was done by supplying a moist synthetic air stream of known water mixing ratio and isotopic composition. The air stream was produced using a nozzle injector (Microdrop GmbH), which injects water droplets of known size (~49 pL) at a preset repetition frequency into a stream of dry nitrogen or synthetic air [32]. Complete evaporation of the small droplets assures that there is no isotopic fractionation between the liquid phase and the generated moist "air". The water mixing ratio is controlled by the repetition rate and dry nitrogen mass flow.

Figure 2 shows the precision of the isotope ratio determination (standard deviation) as a function of averaging time, at a water mixing ratio of 20 ppmv, 350 ppmv and 1300 ppmv. At 1300 ppmv, the standard deviation of the isotope determination is inversely proportional to the square root of the averaging time, down to minimum values of 0.19‰ for $\delta^{18}O$, 0.37‰ for $\delta^{17}O$, and ~1‰ for $\delta^{2}H$, reached at an averaging time of

~25 s. At 350 ppmv, the best standard deviation is 0.37‰ for $\delta^{18}O$ and 0.8‰ for $\delta^{17}O$ obtained with an integration time of 50 s, while deuterium continues to improve, reaching 1.5‰ for an integration time of 200 s. At a water mixing ratio of 20 ppmv, instead, the standard deviations continue to decrease for all isotopes up until the maximum integration time of 200 s. At this point, precisions of 4‰ for $\delta^{18}O$, 22‰ for $\delta^{17}O$, and 54‰ for $\delta^{2}H$ are reached. To summarize, the measurement precision improves with the square root of the averaging time until the limits of instrumental drift are reached. At low mixing ratio the precision of the measurements is limited by the low absorption signals (and thus the signal-to-noise ratio of the line profiles), resulting in a standard deviation that continues to decrease up until the longest averaging times tested (200 s). At the higher mixing ratios, the effect of instrumental drift becomes visible at ever-shorter integration times.

Pre and post-flight calibrations were carried out in the laboratory. Under identical experimental conditions, including identical breadboard temperature, cavity pressure and gas flow, we measured two local water standards GS-48 and GS-50, which are isotopically well-characterized by repeated mass spectrometric analyses. The isotopic compositions are given by: $\delta^{2}H(GS\text{-}48) = -43.3\pm0.3‰$, $\delta^{18}O(GS\text{-}48) = -6.52\pm0.03‰$, $\delta^{2}H(GS\text{-}50) = -276.7\pm0.3‰$, and $\delta^{18}O(GS\text{-}50) = -35.01\pm0.03‰$. Using the two local standards we can perform a two-point isotope scale calibration similar to the VSMOW-SLAP calibration recommended by the International Atomic Energy Agency (IAEA) [33, 34]. For these laboratory measurements, GS-48, introduced at a volume mixing ratio of 1424 ppm, also served as the ‘machine reference’ gas, to calibrate the reference absorbance ratio in the denominator of Eq. (1).

Since we use the integrated absorption coefficients (line area), rather than the line peak intensity at center frequency, the isotope ratio determination should be independent of the cavity pressure (which is stabilized to 98 mbar during the tropospheric part of the flight, but follows the outside pressure above an altitude of approximately 16 km). Also, the OF-CEAS measurements have been shown to be highly linear over a range of water mixing ratios spanning almost three orders of magnitude [32]. We therefore would expect the isotope measurements too, to be practically independent of the water volume mixing ratio. This was indeed observed for the oxygen isotopologues. The deuterium isotope determinations, however, show a non-negligible amount-effect for mixing ratios smaller than ~1500 ppmv. This is illustrated in Figure 3, which shows the measured ('apparent') deuterium isotope ratio as a function of the relative change in the volume mixing ratio υ. As expected, the apparent isotope ratio equals zero for a relative change of 0% of the mixing ratio with respect to the reference mixing ratio υ_{ref} = 1424 ppmv. Also, for positive changes of the mixing ratio, the apparent δ^2H remains equal to zero within the measurement uncertainty. For negative changes in the relative mixing ratio $\Delta\upsilon/\upsilon_{ref}=(\upsilon/\upsilon_{ref}-1)$, a decrease in the measured, apparent δ^*, is observed, which to a good approximation can be fit to a linear function:

$$\delta=\delta^*-\omega\,(\Delta\upsilon/\upsilon_{ref}) \qquad (2)$$

with δ^* the measured, and δ the true δ^2H-value. For the data of Figure 3, the slope was determined to be ω = 182 (±18) ‰. These observations are attributed mostly to the increased importance in the fit of the underlying, non-moving baseline structure in the fit of the very weak deuterium line. The lower the mixing ratio, the more the deuterium line intensity becomes comparable in magnitude to the residual baseline structure, resulting in this case in an increasingly underestimated true line intensity.

Eq. (2) is valid for δ^2H-values close to those of the calibration measurement (i.e., -43.3‰, the value of GS-48). It is not expected (in fact, cannot) hold for very depleted (negative) δ^2H-values, such as the values near -600‰ that were encountered in this study at high altitudes. In a previous study it was shown that a more general (first order) model is given by [35]:

$$\delta = \delta_{\cdot} - \gamma(1+\delta_{\cdot})\cdot(\Delta\upsilon/\upsilon_{ref}) \qquad (3)$$

The data of figure 3 yield a slope of γ = 190 (19)‰. Eq. (3) was used to correct the deuterium data for the amount-effect.

Lastly, we consider the sensitivity of the isotope ratio measurements to variations in the gas temperature. Since the infrared transitions used in this study originate from different ground state energy levels, they exhibit different temperature coefficients. It is easily shown that the isotope ratio measurements are to a very good approximation only sensitive to a temperature differential between the 'sample' and 'reference' measurement (see, e.g., [30]). Our choice of line combinations results in temperature sensitivities of +1.2‰/K, -9.1‰/K, and -8.3‰/K for δ^{18}O, δ^{17}O, and δ^2H, respectively [36]. The isotope ratios are corrected for any variation in gas temperature with respect to the laboratory reference measurements, as measured by a temperature sensor located near the exit of the gas cell. For the vertical isotope profiles presented here in the next section, the measured gas temperature turned out to be initially 0.7 ºC higher than during the laboratory calibration sessions, while during the first part of the flight a smooth temperature decrease of about 0.3 ºC was observed. The corrections that were applied to the data are comparable to or smaller than the measurement uncertainty.

4. Results and discussion

The first part of the AMMA campaign took place in Verona, Italy, from July 24 to July 31, 2006. On July 29, 2006, IRIS had its first successful flight on the Geophysica and acquired spectra during the whole flight. The campaign continued in the month of August in Ouagadougou, Burkina Faso (Central Africa, 12° 22' N, 1° 31' W), where IRIS participated in two local science flights. The first took place on August 7, while the second flight opportunity came on August 13. Here we show the data of August 7, since the August 13 spectra contain spurious spikes. These were traced to an unfortunate software error, introduced by code that was added in an attempt to improve the start-up sequence of the spectrometer, which was conservatively set to commence at 5 km altitude (more in particular, the new sequence shortens the settling time of the flow controller). Otherwise, apart from the breadboard temperature, all subsystems of the IRIS device performed well during the flight series. The noise levels on the housekeeping data (like the temperature of the breadboard, and flow and pressure inside the cavity) were similar to those observed during laboratory tests and during the first flight in Verona, indicating that there were no interference problems with other instruments on the airplane (scientific or other).

Figure 4 shows the water vapor measurements during part of the flight of Aug. 7, 2006. We observe volume mixing ratio values above 100 ppm in the troposphere, which decrease rapidly with altitude. An approximate tropopause location at 15 - 17 km was determined from the observed temperature profile. The lowest observed value in the stratosphere was about 10 ppm. Although elevated stratospheric water concentrations were observed also during some July 2005 flights above the North American continent [18], such anomalously high concentrations are not expected in July above central Africa. In fact, the dedicated FISH hygrometer operated by the

German team from Jülich [37], observed more characteristic values in the range of 3 to 6 ppmv. We therefore believe that our results are indicative of slow outgassing of the inlet, which was not heated nor surface treated. Considering the volume of the optical cell (ca. 10 mL) and the flow passing through the cell (150 mL/min), the time needed to exchange the gas volume of the cell is about 4 sec. Furthermore, we previously determined the time response of IRIS only (i.e., without the inlet) to follow an exponential decay with a response time of about 2 s (with a flow rate of ~400 mL/min) [24]. Another indication comes from the observation of slowly, but continuously, decreasing water mixing ratio measurements during the level stratospheric parts of the flight.

The observed outgassing is a concern because it not only affects the measured water volume mixing ratio, but also because the measured isotope ratios may not be representative of the sampled outside air. This is an important reason we did not consider measurements with a water mixing ratio below 100 ppmv in the current analysis. For υ = 100 ppm the effect on the measured isotope ratio is expected to be at most 5% of the actual δ-value, and decreases approximately linearly with increasing mixing ratio. Another reason is that below about 100 ppmv the instrumental noise quickly becomes excessive. At a mixing ratio of 100 ppmv, the precisions are about 9‰, 20‰, and 100‰ in a 1 Hz bandwidth, for $\delta^{18}O$, $\delta^{17}O$, and $\delta^{2}H$ respectively. Longer averaging of the data should enable the same level of precision to be maintained all the way down to stratospheric water concentration levels. The laboratory measurements of Figure 2a show that this is in principle possible up to an effective averaging time of at least 200 s. However, the stratospheric measurements (p < 98 mbar, altitude > 16 km, υ < ~30 ppmv) of this study are compromised by the absence of pressure stabilization. Through modulation of the refractive index,

pressure changes will move the cavity mode structure (which is used to sample the spectrum at equidistant frequencies, spaced by the cavity free spectral range), as well as the underlying residual optical fringe structure. This in turn results in a reduction of the effectiveness of the applied averaging in the spectral fit procedure. In-flight breadboard temperature (gradient) changes can also result in a moving cavity mode structure. Together these effects result in a standard deviation of the isotope measurement that does not improve with averaging beyond a few seconds at low altitudes and as little as one to two seconds in the stratosphere. Hence, the data shown here is averaged for 1 second only.

As can be seen from the lower panel of Figure 4, the instrument temperature is initially stable, but starts to decrease during the ascent of the airplane. Once level altitude has been reached, it takes almost 2 hours before a new equilibrium temperature is reached. The approximately 85 ºC lower outside temperature (-50 ºC versus +35 ºC on departure) results in a 5 ºC lower average breadboard temperature. This is sufficient to cause a small but noticeable misalignment of the optics, resulting in a decrease of the detector signals by a factor of almost two. This is the reason the data recorded during descent of the airplane is not shown.

Figure 5 shows vertical isotope-ratio profiles versus the water mixing ratio, for the first 10 minutes of the flight of Aug 7, 2006, where the altitude ranges from 7.7 to 11 km (potential temperature in the range from approximately 330 K to 370 K). As expected, a gradual depletion in heavy isotopologues is observed with increasing altitude. In the same figure the data are compared to model calculations of one-dimensional Rayleigh distillation of an isolated air mass. We apply the Rayleigh model in its most simple form, as first described by Dansgaard [14] and discussed by, e.g., Jouzel [15]:

$$\delta_v = (1+\delta_0)\cdot(\upsilon/\upsilon_0)^{\alpha(T)-1} - 1 \quad (4)$$

Here, δ_0 and δ_v are the initial and the final isotope ratios of the water vapor and υ and υ_0 are the initial and final water vapor mixing ratio. $\alpha(T)$ is the fractionation factor at the mean temperature $(T+T_0)/2$. The fractionation factors are taken from Majoube for oxygen-18 [38], and from Merlivat and Nief for deuterium [39]. Values for α are approximately 1.0087 for ^{18}O and 1.0701 for ^{2}H at 307 K, being the temperature of the air at 0.3 km (the altitude of the airport in Ouagadougou), and increase slowly as temperature decreases. The choice of the starting values for δ_0, is slightly problematic. In fact, no vapor isotope values have been published for the same geographical location and time of year. One choice could be to use the isotope values determined with our own spectrometer. Instead, in order to retain as much the *ab initio* character of the Rayleigh distillation curve, we have chosen to use mean precipitation values for the month of August collected in 1989 at the station of Barogo, ca. 13 km NE of Ouagadougou airport, altitude 280 m. These values, as reported in the Global Network on Isotopes in precipitation (GNIP) [40] database, are –34.5‰ for δ^2H and –5.4‰ for $\delta^{18}O$ and are in good agreement with the (interpolated) weighted August mean precipitation values reported by the GNIP Maps and Animations Project [41]. The corresponding vapor phase isotope ratios are obtained by assuming isotopic equilibrium between condensate and vapor phase. The Rayleigh curves can thus be determined with a starting isotopic composition of the water vapor given by $\delta^2H_0 = -98$ ‰ and $\delta^{18}O_0 = -14$ ‰. It should be noted that the upper troposphere isotope ratios predicted by the Rayleigh model are not very sensitive to these starting value. Instead, the upper troposphere values are mostly determined by the fractionation factors, and thus largely controlled by the atmospheric temperature profile. The final assumption

is that of a constant relative humidity h at all vertical levels, leading to the following expression for the volume mixing ratio:

$$\upsilon = \frac{h \cdot e_w(T)}{p} \tag{5}$$

where p is the total pressure and $e_w(T)$ is the saturation vapor pressure approximated by [9]:

$$e_w(T) = e_0 \cdot e^{(-\frac{b}{T})} \tag{6}$$

with T the temperature in K, $e_0 = 3.5753 \cdot 10^{10}$ hPa, and $b = 6142$ K for saturation over ice. The temperature T and the atmospheric pressure p were taken from meteorological sensors onboard of the Geophysica airplane. Finally, the Rayleigh curves for $\delta^{17}O$ have been determined using the mass-dependent relationship between tropospheric $\delta^{17}O$ and $\delta^{18}O$, as established by Meijer and Li [42].

The results are shown as the solid lines in Figure 5. The Rayleigh curves generally overestimate the degree of depletion of the atmospheric moisture, in accordance with previous in-situ observations [17, 18]. This is to be expected as the open system, Rayleigh model does not allow for the condensed phase to remain in the cloud. Also, this simple model does not take into account turbulent mixing during the transport of the air masses and other complexities of the hydrological cycle (see, e.g. [43]). Departure from the temperature-controlled Rayleigh distillation at higher altitudes (in the low TTL) to less negative delta-values, for which the data of Figure 5 gives some indication, is clearly evident in the TTL data of the Atmospheric Trace Molecule Spectrometry (ATMOS; [11]) and the Atmospheric Chemistry Experiment Fourier Transform Spectrometer (ACE-FTS; [44]) satellite-based instruments. It is also seen in the in-situ data set of Webster and Heymsfeld [17] and the Harvard ICOS instrument [18]. It can be interpreted as evidence of convective ice-lofting to altitudes

below the cold point (level of lowest saturation mixing ratio) [45]. However, it may be clear that the noise level on the current 1-second averaged dataset, as well as its limited extend, do no warrant any firm conclusions about upper tropospheric processes influencing the isotope profiles.

As already mentioned in the Introduction, the WAS instrument of the Utrecht group did not yield valid water isotope data during this campaign. Comparison with their published $\delta^{17}O$ and $\delta^{18}O$ data of August 2004 is not appropriate because those data were collected at high southern latitude (65º S) and mixing ratios below 50 ppmv, even though the range of tropospheric values observed by Franz and Röckmann [19] ($-90‰ < \delta^{18}O < -30‰$, $-50‰ < \delta^{17}O < -10‰$) is similar to that of this study.

Although the smoothed oxygen isotope profiles do not coincide with the respective Rayleigh curves, the low altitude (1600 ppmv) values of $\delta^{17}O = –33.5‰$ and $\delta^{18}O = –62‰$ are in good agreement with the assumption of mass dependent fractionation. This gives some confidence in the internal consistency of the isotope ratio calibration. However, it should be noted that the error on the $\delta^{17}O$ and $\delta^{18}O$ measurements is not strongly correlated (as is the case with the measurements of Franz and Röckmann [19]), leading to a larger error on the calculated ^{17}O-anomaly $\Delta^{17}O = (\mathrm{Ln}(1+\delta^{17}O) – 0.528 \cdot \mathrm{Ln}(1+\delta^{18}))$ [42, 46]. Whereas for the data with 1200 ppm $< \upsilon <$ 1600 ppmv, $\Delta^{17}O = 0 \pm 5‰$, the average over all data (100 ppmv $< \upsilon <$ 1600 ppmv) equals $+1 \pm 15‰$, with the errors representing one standard deviation. These results, shown in Figure 6, are in agreement with the observation by Franz and Röckmann of a zero anomaly in the troposphere and a zero or very small anomaly ($|\Delta^{17}O| < 2‰$) in the low stratosphere.

In Figure 7 the deuterium data of Figure 5 are plot against the corresponding ^{18}O measurements. For reference, the Rayleigh curve and the Global Meteoric Water Line

(GMWL: $\delta^2H = 8\ \delta^{18}O + 10‰$, a relation approximately obeyed by water isotopes in precipitation in the low troposphere [see, e.g., 47]) are shown. This figure demonstrates the largely non-correlated nature of the measurement errors. We thus conclude that the spread in the measurements seen in Figure 5 is predominantly instrumental and not caused by natural variations in the isotopic composition of the air. Although both Webster and Heymsfeld [17], and Hanisco and co-workers [18] have measured both δ^2H and $\delta^{18}O$, neither of them has published the experimentally observed $\delta^2H - \delta^{18}O$ relation.

5. Conclusions and Perspectives

We have illustrated the airborne deployment of a new spectroscopic technique for in situ detection of the isotopic composition of water vapor in the upper troposphere and the lower stratosphere onboard of the M55 Geophysica high altitude platform. Although the noise level of the data leaves room for improvement and the data are limited to the upper troposphere, the $\Delta^{17}O$ data and the δ^2H-$\delta^{18}O$ relation are the first such results published, obtained with an aircraft-based, in-situ spectrometer. The observation of $\Delta^{17}O=0$ in the TTL is in agreement with the previous measurement by Franz and Röckmann [19].

The experimental results obtained so far are important because they demonstrate that in principle such a setup can work on a stratospheric aircraft. The experience will also guide further development of the spectrometer. The next generation of the spectrometer has been equipped with a heating system in which each heater is equipped with its own temperature sensor and control loop. Initial experiments indicate that six sensors, strategically distributed over the setup, suffice to control the temperature of the optical head to a high degree of uniformity. This resolves the major

engineering problem encountered during this campaign and should enable data integration over time scales up to ~100 s, providing an order of magnitude improvement in measurement precision, also under flight conditions in the tropics.

Furthermore, the prospect of extending the OF-CEAS technique to longer wavelengths is very promising. A move towards the fundamental vibrational stretching band of water near 2.6 μm should improve the measurements precision by one more order of magnitude. In Figure 8 the experimentally determined measurement precision of the current near-infrared (NIR) spectrometer is shown as a function of the water volume mixing ratio with 200-s data averaging. The figure also shows the predicted level of precision of the same spectrometer operating in the 2.6 μm region. The water absorptions excited at the longer wavelength are close to those we worked with in our early laboratory spectrometer [35], and on average they are one order of magnitude stronger (a factor of 40 for HO^2H, 15 for $H^{17}OH$, 6 for $H^{18}OH$, and 20 for $H^{16}OH$) than the NIR transitions. The laser source is a near room temperature InAs DFB laser with an output power > 3 mW (Nanoplus). Apart from the laser source, the CRD mirrors need to be changed. A trial coating run resulted in mirrors that perform a factor of only two worse (in terms of ring-down time) than the NIR mirrors. Contrary to most other implementations of CEAS (including OA-ICOS), the OF-CEAS technique is characterized by an extremely high light transmission through the cavity (higher by a factor of roughly $1/(1-R) > 10^4$, with R the mirror reflectivity), such that detector performance is not a limiting factor. It therefore seems probable that an instrument sensitivity in the 10^{-10} $cm^{-1}/\sqrt{Hz}$ range can be realized. As Figure 8 indicates, this level of performance in the MIR, together with an effective data averaging of the order of 100 s, would yield precisions of about 3‰ (deuterium) and better (the $\delta^{17}O$ and $\delta^{18}O$ isotope ratios) at a stratospheric mixing ratio of 10

ppmv. Of course, this predicted performance might not be met entirely in practice. Notably, the new instrument will operate at a cavity pressure below the lowest outside pressure of ca. 65 mbar encountered in the low stratosphere, reducing the number density of water molecules. On the positive side, the lower pressure reduces the gas exchange time, especially as on future missions the spectrometer will be operated at a roughly three times higher flow rate (~0.5 SL/min). Together this shortens the response time by a factor of about 6 and this is expected to significantly reduce memory effects. With these measures, such a spectrometer would meet or surpass the performance of the current line of airborne, in-situ water isotope spectrometers [17, 18], without the use of cryogens, and with a much reduced power consumption and size.

Acknowledgements

This work was supported by the Dutch Foundation for Fundamental Research on Matter (FOM) project 99MAP10, the EC EUFAR Transnational Access program, and NASA. It used the infrastructure of the AMMA/SCOUT-03 campaign.

The authors are very grateful to Henk Been, Jeff Grose and Bruce Borchers for their excellent technical assistance. Thanks are owed as well to the COLD team: Silvia Viciani, Francesco Castagnoli, Alessio Montori, and Piero Mazzinghi; for their support with the integration of IRIS on the CVI-rack, and for sharing their in-the-field infra-structure and know-how with us during the Verona and Ouagadougou campaigns. We want to thank the WAS-team in particular for their collaboration, and all AMMA teams present in Ouagadougou for their help, support, flexibility, and without exception very pleasant cooperation.

Finally, we thank Francesco Cairo, Cornelius Schiller, and two anonymous reviewers for valuable comments on the manuscript.

References

[1] Rosenlof K. H., Oltmans S. J., Kley D., Russell III J. M., Chiou E.-W., Chu W. P., Johnson D. G., Kelly, K. K., Michelsen H. A., Nedoluha G. E., Remsberg E. E., Toon G. C., and Mc- Cormick M. P., Stratospheric water vapor increases over the past half-century. *Geophys. Res. Lett.*, ***28***, 1195–1198 (2001).

[2] Forster P. M., Shine K. P., Assessing the climate impact of trends in stratospheric water vapor. *Geophysical Research Letters*, **29**, 1086 (2002).

[3] Kirk-Davidoff D. B., Anderson J. G., Hintsa E. J., and Keith D. W., The effect of climate change on ozone depletion through changes in stratospheric water vapor. *Nature*, **402**, 399-401 (1999).

[4] Dessler A. E., A reexamination of the "stratospheric fountain" hypothesis. *Geophys. Res. Lett., **25,*** 4165-4168 (1998).

[5] Kaye J. A., Analysis of the origins and implications of the ^{18}O content of stratospheric water vapor. *J. Atmos. Chem.*, ***10***, 39– 51 (1990).

[6] Moyer E. J., Irion F. W., Yung Y. L., Gunson M. R., ATMOS stratospheric deuterated water and implications for troposphere-stratosphere transport. *Geophys. Res. Lett.*, **23** (17), 2385-2388 (1996).

[7] Keith W., Stratospheric-tropospheric exchange: Inferences from the isotopic composition of water vapor. *J. Geophys. Res.*, **105**, 15167-15174 (2000).

[8] Sherwood S. C., and Dessler A. E., A model for transport across the tropical tropopause. *J. Atmos. Sci.*, ***58***, 765–779 (2001).

[9] Johnson D. G., Jucks K. W., Traub W. A., and Chance K. V., Isotopic composition of stratospheric water vapor: Implications for transport. *J. Geophys. Res*., ***D106***, 12211-12218 (2001); *ibid,* 12219-12226 (2001).

[10] Dessler A. E., and Sherwood S. C., A model of HDO in the tropical tropopause layer. *Atmos. Chem. Phys.*, ***3***, 2173-2181 (2003).

[11] Kuang Z., Toon G. C., Wennberg P. O., and Yung Y. L., Measured HDO/H_2O ratios across the tropical tropopause. *Geophys. Res. Lett.*, ***30(7)***, 1372 (2003).

[12] Bechtel C., and Zahn A., The isotope composition of water vapour: A powerful tool to study transport and chemistry of middle atmospheric water vapour. *Atmos. Chem. Phys.*, *3*, 3991–4036 (2003).

[13] Clark I. D., and Fritz P., Environmental Isotopes in Hydrogeology. CRC Press, Boca Raton, FL (1997).

[14] Dansgaard W., Stable isotopes in precipitation. *Tellus*, **16**, 436-438 (1964).

[15] Jouzel J., Isotopes in cloud physics: Multistep and multistage processes. *The Terrestrial Environment B,* P. Fritz and J. C. Fontes, Eds., Vol. 2, *Handbook of Environmental Isotopes Geochemistry,* Elsevier, 61–112. (1986).

[16] Holton J. R., and Gettelman A., Horizontal transport and the dehydration of the stratosphere. *Geophys. Res. Lett.*, ***28***, 2799–2802 (2001).

[17] Webster C. R., and Heymsfield A., Water Isotope Ratios D/H, $^{18}O/^{16}O$, $^{17}O/^{16}O$ in and out of Clouds Map Dehydration Pathways. *Science*, ***302***, 1742-1745 (2003).

[18] Hanisco T. F., and Coauthors, Observations of deep convective influence on stratospheric water vapor and its isotopic composition. *Geophys. Res. Lett.*, ***34***, L04814, doi:10.1029/2006GL027899 (2007).

[19] Franz P., and Röckmann Th., High-precision isotope measurements of $H_2{}^{16}O$, $H_2{}^{17}O$, $H_2{}^{18}O$, and the $\Delta^{17}O$-anomaly of water vapor in the southern lowermost stratosphere. *Atmos. Chem. Phys*., ***5***, 2949-2959 (2005).

[20] Zahn A., Barth V., Pfeilsticker K., and Platt U., Deuterium, Oxygen-18 and tritium as tracers for water vapour transport in the lower stratosphere and tropopause region. *J. Atmos. Chem.*, ***30***, 25–47 (1998).

[21] Steinwagner J., Milz M., von Clarmann T., Glatthor N., Grabowski U., Höpfner M., Stiller G. P., and Röckmann Th., Global HDO measurements with MIPAS. *Atmos. Chem. Phys.*, *7*, 2601-2615 (2007).

[22] Sayres, D. S., Moyer E. J., Hanisco T. F., St. Clair J. M.,. Keutsch F. N, O'Brien A., Allen N. T., Lapson L., Demusz J. N., Rivero M., Martin T., Greenberg M., Tuozzolo C., Engel G. S., Kroll J. H., Paul J., and Anderson J. G, A new cavity based absorption instrument for the detection of water isotopologues in the upper troposphere and lower stratosphere (March 28, 2008). http://www.arp.harvard.edu/atmobs/sciobj/instrument/IcosInstrumentPaper.pdf

[23] Moyer E. J., Sayres D. S., Engel G. S., St. Clair J. M., Keutsch F. N., Allen N. T., Kroll J. H., Anderson J. G., Design considerations in high-sensitivity off-axis integrated cavity output spectroscopy. *Appl. Phys. B*, **92(3)**, 467-474 (2008).

[24] Kerstel E. R. Th., Iannone R. Q., Chenevier M., Kassi S., Jost H.-J., and Romanini D., A Water Isotope (^2H, ^{17}O, and ^{18}O) Spectrometer based on Optical-Feedback Cavity Enhanced Absorption For *In-situ* Airborne Applications. *Appl. Phys. B*, **85(2-3)**, 397-406 (2006).

[25] Morville J., Kassi S., Chenevier M., and Romanini D., Fast, low–noise, mode–by–mode, cavity–enhanced absorption spectroscopy by diode–laser self–locking. *Appl. Phys. B*, **80**, 1027-1038 (2005).

[26] Dessler A. E., Minschwaner K., An analysis of the regulation of tropical tropospheric water vapor. *J. Geophys. Res*., **112**, D10120, doi: 10.1029/2006JD007683 (2007).

[27] Franz P., and Röckmann Th., A new continuous flow isotope ratio mass spectrometry system for the analysis of δ^2H, $\delta^{17}O$ and $\delta^{18}O$ of small (120 μg) water samples in atmospheric application. *Rapid Commun. Mass Spectrom*., **18**, 1429–1435 (2004).

[28] Viciani S., D'Amato F., Mazzinghi P., Castagnoli F., Toci G., and Werle P., A cryogenic operated diode-laser spectrometer for airborne measurement of stratospheric trace gases. *Appl. Phys. B* ***90***, 581-592 (2008).

[29] Rothman L. S., and co-authors, HITRAN molecular database. *J. Quant. Spectrosc. Radiat. Transf.*, **96**, 139-204 (2005).

[30] Kerstel E. R. Th., Isotope Ratio Infrared Spectrometry, in *Handbook of Stable Isotope Analytical Techniques*, ed. P.A. de Groot, Elsevier , chapter 34, pp. 759–787, Elsevier, Amsterdam. (2004).

[31] Gonfiantini R., Standards for stable isotope measurements in natural compounds. *Nature*, **271**, 534-536 (1978).

[32] Iannone R. Q., Romanini D., Kassi S. , Meijer H. A. J., and Kerstel E. R. T., A microdrop generator for the calibration of a water vapor isotope ratio spectrometer. *J. Atmos. Ocean. Technol.* (accepted, 2008). doi: 10.1175/2008JTECHA1218.1

[33] Hut G., Report to the Director General, International Atomic Energy Agency, Vienna (1987).

[34] Gonfiantini R., Advisory Group Meeting on Stable Isotope Reference Samples for Geochemical and Hydrological Investigations; IAEA: Vienna. (1984).

[35] Kerstel E. R. Th., van Trigt R., Dam N., Reuss J., Meijer H. A. J., Simultaneous determination of the $^{2}H/^{1}H$, $^{17}O/^{16}O$, and $^{18}O/^{16}O$ isotope abundance ratios in water by means of laser spectrometry. *Anal. Chem.* **71**, 5297-5303 (1999).

[36] Kerstel E. R. Th., Gagliardi G., Gianfrani L., Meijer H. A. J., van Trigt R., Ramaker R., Determination of the $^{2}H/^{1}H$, $^{17}O/^{16}O$, and $^{18}O/^{16}O$ isotope ratios in water by means of tunable diode laser spectroscopy at 1.39 μm. *Spectrochimica Acta Part A*, **58**, 2389-2396 (2002).

[37] Kiemle C., Wirth M., Fix A., Ehret G., Schumann U., Gardiner T., Schiller C., Sitnikov N., and Stiller G. First airborne water vapor lidar measurements in the tropical upper troposphere and mid-latitudes lower stratosphere: accuracy evaluation and intercomparison with other instruments. *Atmos. Chem. Phys*., **8**, 5245–5261 (2008).

[38] Majoube M., Fractionnement en oxygène-18 et en deutérium entre l'eau et sa vapeur. *Jour. Chem. Phys*., **197**, 1423-1436 (1971).

[39] Merlivat L. and Nief G., Fractionnement isotopique lors de changement d'état solide-vapeur et liquide-vapeur de l'éau a des temperatures à 0°C. *Tellus*, **19**, 122-127 (1967).

[40] IAEA/WMO, Global Network of Isotopes in Precipitation. The GNIP Database. Accessible at http://isohis.iaea.org. (2006).

[41] IAEA, GNIP Maps and Animations, International Atomic Energy Agency, Vienna. Accessible at http://isohis.iaea.org. (2001).

[42] Meijer H., and Li W., The use of electrolysis for accurate ^{17}O and ^{18}O isotope measurements in water isotopes. *Isotopes Environ. Health Stud.,* **34**, 349–369 (1998).

[43] Sturm K., Hoffmann G., Langmann B., and Stichler W., Simulation of $\delta^{18}O$ in precipitation by the regional circulation model REMOiso. *Hydrol. Processes,* **19,** 3425–3444 (2005).

[44] Nassar R., Bernath P. F., Boone C. D., Gettelman A., McLeod S. D., and Rinsland C. P., Variability in HDO/H_2O abundance ratios in the tropical tropopause layer. *J. Geophys. Res.*, **112**, D21305, doi: 10.1029/2007JD008417 (2007).

[45] Dessler A. E., Hanisco T. F., Fueglistaler S., Effects of convective ice lofting on H_2O and HDO in the tropical tropopause layer. *J. Geophys. Res.*, **112**, D18309, doi: 10.1029/2007JD008609 (2007).

[46] Young E. D., Galy A., Nagahara H., Kinetic and equilibrium mass-dependent isotope fractionation laws in nature and their geochemical and cosmochemical significance. *Geochim. Cosmochim. Acta,* **66**, 1095 –1104 (2002).

[47] Mook W.G., Environmental Isotopes in Hydrological Cycle, Principles and Applications, Vol 1. IAEA. (2000).

Figure Captions

Figure 1. A typical in-flight spectrum recorded in approx 0.16 s during ascent of the August 7 flight from Ouagadougou at a height of approximately 10 km (water mixing ratio ~ 300 ppm). The top-panel shows the spectrum (open circles). The solid curve is

a best fit to the spectrum, as explained in the text. The residual of the fit is shown in the bottom panel. The RMS deviation amounts to 6.6 10^{-10} cm^{-1}.

Figure 2. Measurement precision (as given by the standard deviation) versus averaging time during laboratory operation of the IRIS spectrometer at water mixing ratios of 20 ppmv (a), 350 ppmv (b) and 1300 ppmv (c), respectively. The analysis demonstrates that the optimum integration time is about 200 s at the lowest water mixing ratios, but at higher water mixing ratios is limited by instrumental drift (indicated by the positively sloping straight line sections in the figures; ^{18}O (– – –), ^{17}O (——), and ^{2}H (▪▪▪▪)). At 1300 ppmv and 25 s averaging, precision levels of about 0.2‰, 0.5‰, and 1‰ are reached for $\delta^{18}O$ (◊), $\delta^{17}O$ (●), and $\delta^{2}H$ (□), respectively.

Figure 3. Influence of the relative water vapor mixing ratio variation on the measured (a) $\delta^{2}H$, (b) $\delta^{17}O$, and (c) $\delta^{18}O$ values. The reference volume mixing ratio equals 1424 ppmv (close to the maximum value of the isotope profiles of Figure 5). The weighted linear fit to the data (solid curve) is used to correct the actual deuterium flight data. The correction for positive relative variations in the mixing ratio was measured to be zero within the measurement uncertainty, also for deuterium.

Figure 4. Water mixing ratio (solid line) and altitude (dashed line) during the flight of Aug. 7, 2006. In the lower panel, the temperatures of the optical breadboard (1) and of the optical cell (2) are shown. Total flight duration was approximately 4 hours. The section from 606 to 616 min is used to produce the vertical profiles of Fig. 5.

Figure 5. (a) δ^2H, (b) $\delta^{17}O$, and (c) $\delta^{18}O$ against the water vapor mixing ratio for a tropospheric section of the flight of August 7, 2006, near 12° 22' N and 1° 31' W. The data are averaged for 1 s. The continuous lines passing through the data are smoothed profiles and only serve to guide the eye. Rayleigh curves (black continuous lines) are shown for comparison.

Figure 6. The ^{17}O-anomaly as a function of water vapor mixing ratio for the data of Figure 5. The tropospheric data with 1200 ppm < υ < 1600 ppm have $\Delta^{17}O = 0 \pm 5‰$, whereas the mean for all data equals $+1 \pm 15‰$, in agreement with the expectation of mass-dependent fractionation in the troposphere.

Figure 7. δ^2H against $\delta^{18}O$ for tropospheric water vapor during the flight of August 7, 2006. The open circles are data averaged for 1 s, whereas the full squares represent 10 s averages. The dashed line represents the Global Meteoric Water Line (GMWL) for precipitation, and the continuous line is the prediction based on the Rayleigh distillation model.

Figure 8. Experimental (NIR) and predicted (MIR) precision of the isotope ratio measurements as a function of the water mixing ratio. The experimental data is for the NIR (1.4 μm) spectrometer with an effective data averaging time of 200 s. The higher absorption line strengths in the MIR (2.6 μm) translate into higher detection sensitivity, or better measurement precision at the same water concentration level, as indicated by the solid curves.

Figures

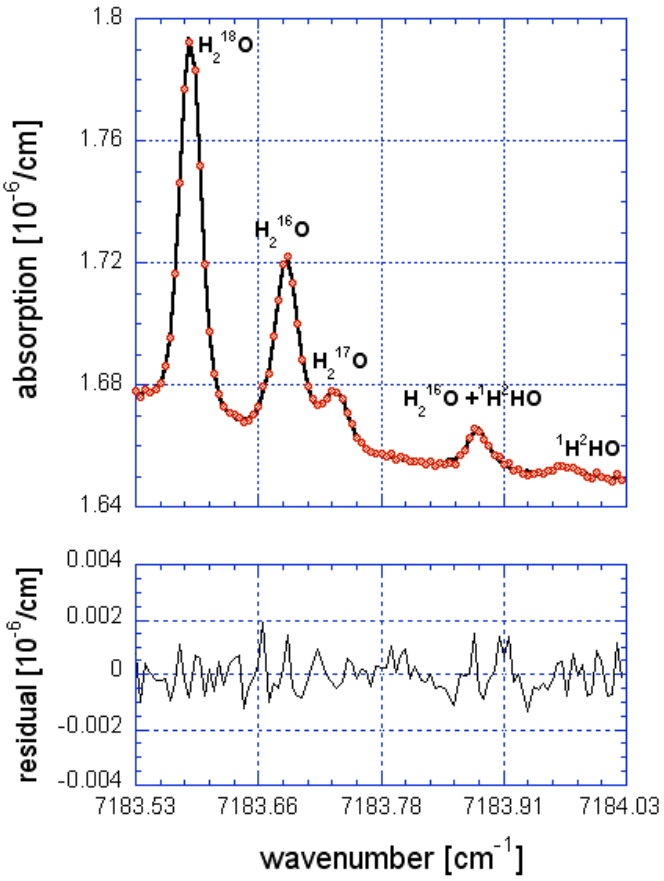

Figure 1. A typical in-flight spectrum recorded in approx 0.16 s during ascent of the August 7 flight from Ouagadougou at a height of approximately 10 km (water mixing ratio ~ 300 ppm). The top-panel shows the spectrum (open circles). The solid curve is a best fit to the spectrum, as explained in the text. The residual of the fit is shown in the bottom panel. The RMS deviation amounts to 6.6 10^{-10} cm^{-1}.

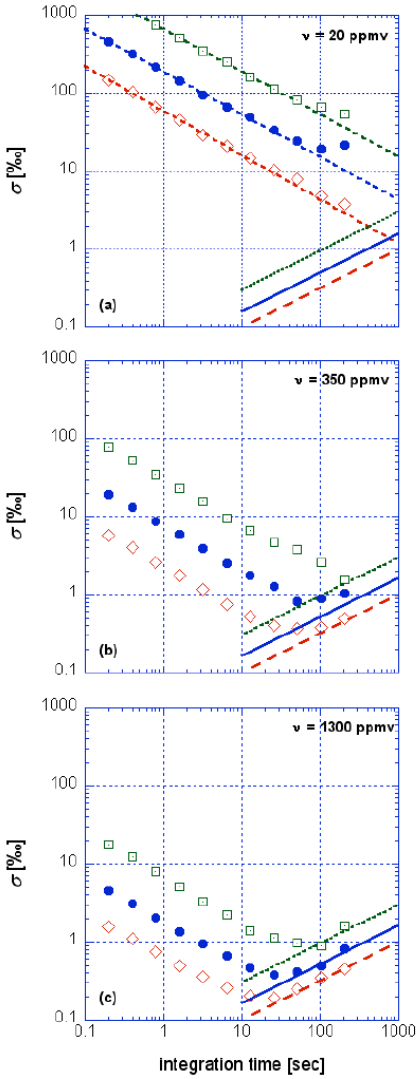

Figure 2. Measurement precision (as given by the standard deviation) versus averaging time during laboratory operation of the IRIS spectrometer at water mixing ratios of 20 ppmv (a), 350 ppmv (b) and 1300 ppmv (c), respectively. The analysis demonstrates that the optimum integration time is about 200 s at the lowest water mixing ratios, but at higher water mixing ratios is limited by instrumental drift (indicated by the positively sloping straight line sections in the figures; ^{18}O (– – –), ^{17}O (——), and ^{2}H (▪▪▪▪)). At 1300 ppmv and 25 s averaging, precision levels of about 0.2‰, 0.5‰, and 1‰ are reached for $\delta^{18}O$ (◊), $\delta^{17}O$ (●), and $\delta^{2}H$ (□), respectively.

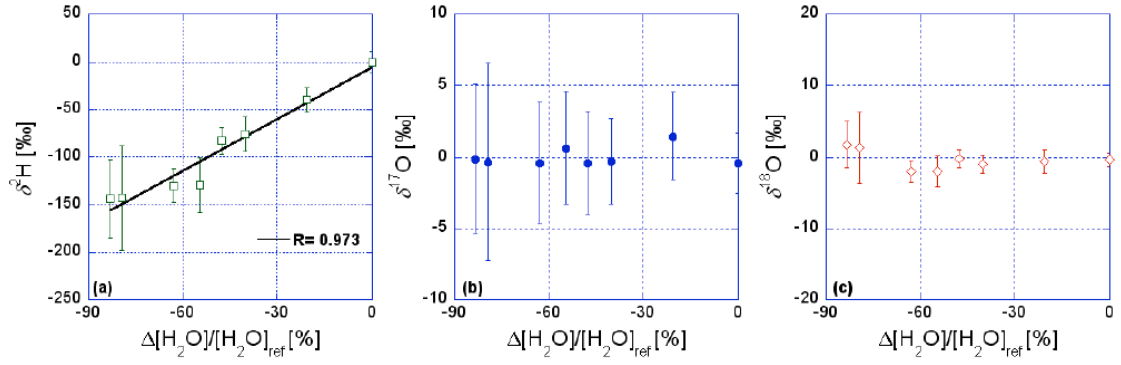

Figure 3. Influence of the relative water vapor mixing ratio variation on the measured (a) δ^2H, (b) δ^{17}O, and (c) δ^{18}O values. The reference volume mixing ratio equals 1424 ppmv (close to the maximum value of the isotope profiles of Figure 5). The weighted linear fit to the data (solid curve) is used to correct the actual deuterium flight data. The correction for positive relative variations in the mixing ratio was measured to be zero within the measurement uncertainty, also for deuterium.

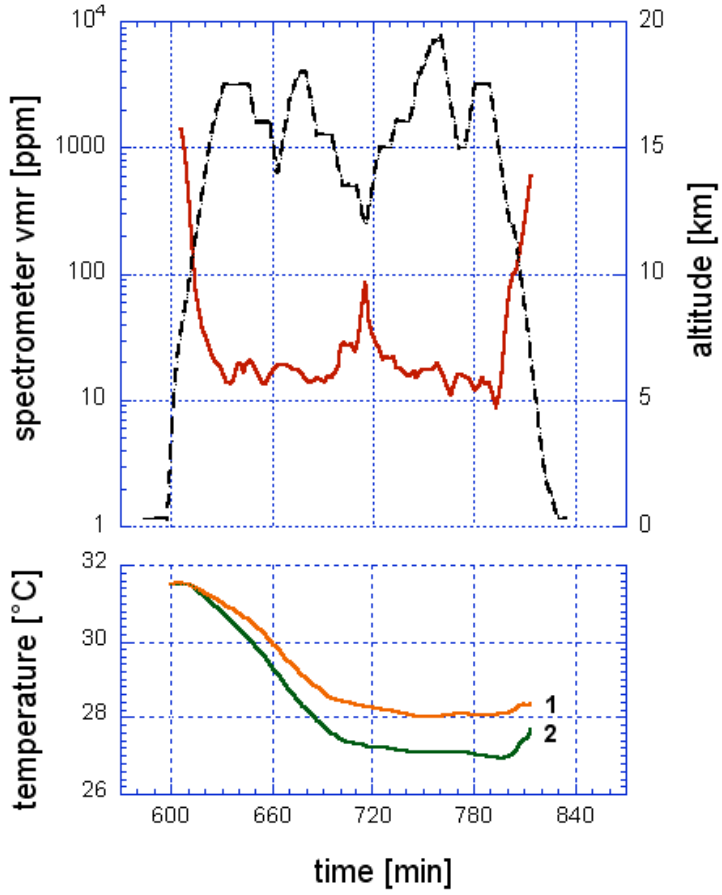

Figure 4. Water mixing ratio (solid line) and altitude (dashed line) during the flight of Aug. 7, 2006. In the lower panel, the temperatures of the optical breadboard (1) and of the optical cell (2) are shown. Total flight duration was approximately 4 hours. The section from 606 to 616 min is used to produce the vertical profiles of Fig. 5.

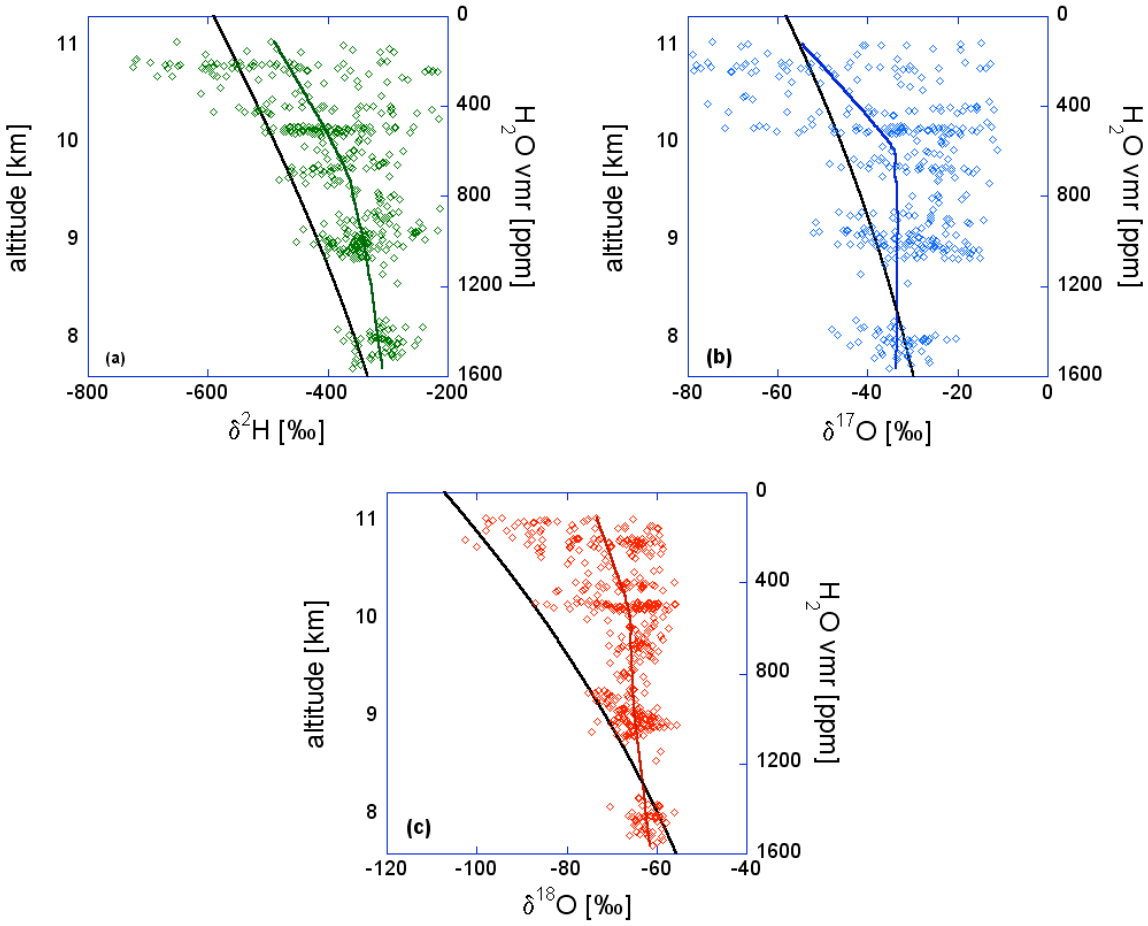

Figure 5. (a) δ^2H, (b) $\delta^{17}O$, and (c) $\delta^{18}O$ against the water vapor mixing ratio for a tropospheric section of the flight of August 7, 2006, near 12° 22' N and 1° 31' W. The data are averaged for 1 s. The continuous lines passing through the data are smoothed profiles and only serve to guide the eye. Rayleigh curves (black continuous lines) are shown for comparison.

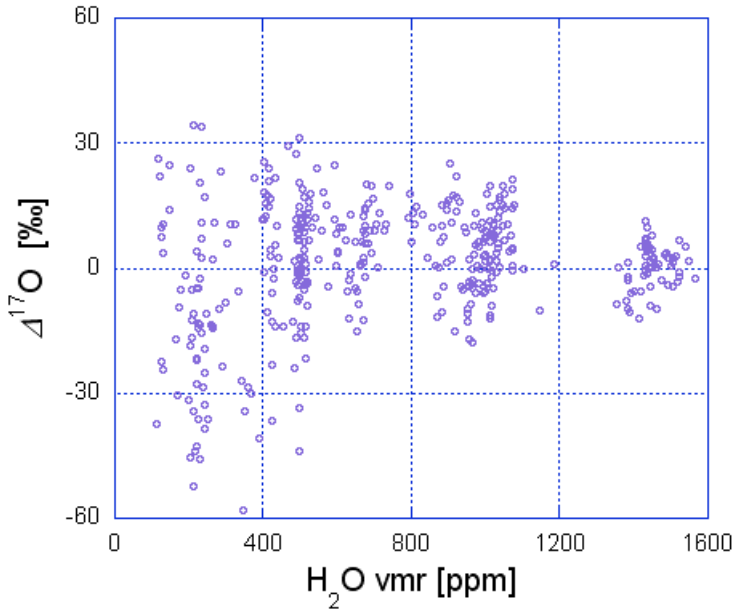

Figure 6. The ^{17}O-anomaly as a function of water vapor mixing ratio for the data of Figure 5. The tropospheric data with 1200 ppm < υ < 1600 ppm have $\Delta^{17}O = 0 \pm 5‰$, whereas the mean for all data equals +1 ± 15‰, in agreement with the expectation of mass-dependent fractionation in the troposphere.

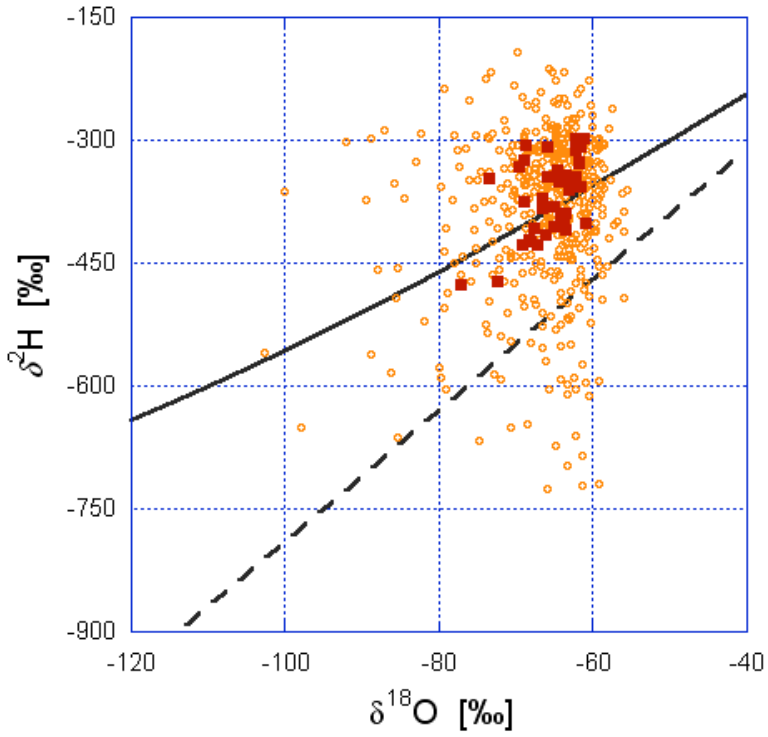

Figure 7. δ^2H against $\delta^{18}O$ for tropospheric water vapor during the flight of August 7, 2006. The open circles are data averaged for 1 s, whereas the full squares represent 10 s averages. The dashed line represents the Global Meteoric Water Line (GMWL) for precipitation, and the continuous line is the prediction based on the Rayleigh distillation model.

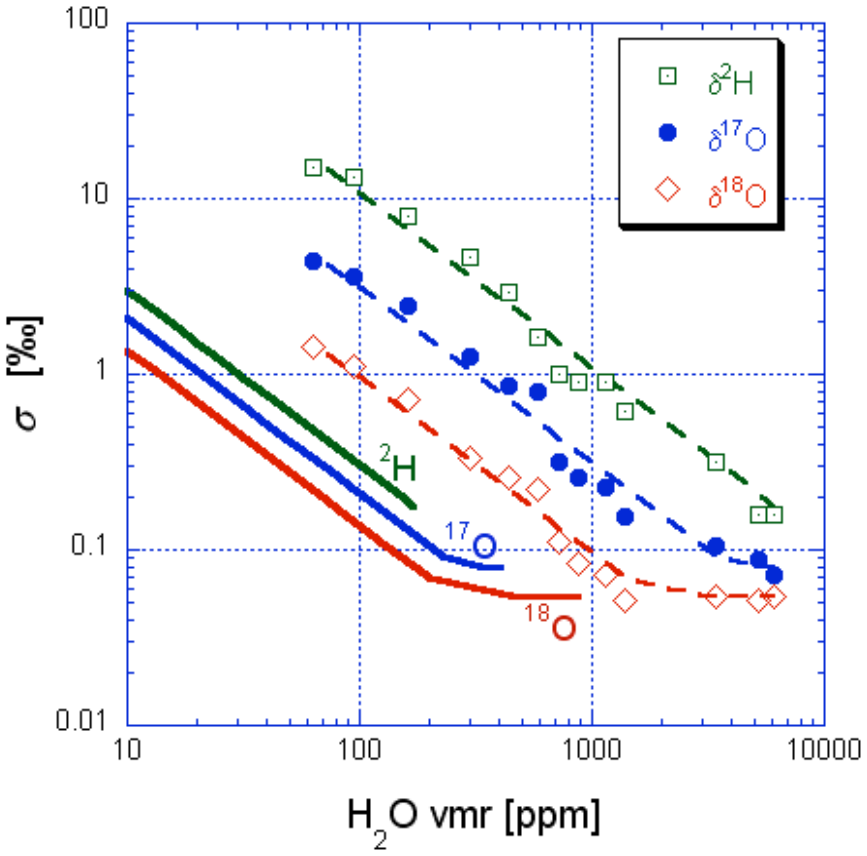

Figure 8. Experimental (NIR) and predicted (MIR) precision of the isotope ratio measurements as a function of the water mixing ratio. The experimental data is for the NIR (1.4 μm) spectrometer with an effective data averaging time of 200 s. The higher absorption line strengths in the MIR (2.6 μm) translate into higher detection sensitivity, or better measurement precision at the same water concentration level, as indicated by the solid curves.